Molecular-level effects on cell membrane models to explain the phototoxicity of gold shell-isolated nanoparticles to cancer cells

Sabrina A. Camacho[1,2], Mirella B. Kobal[1], Alexandre M. Almeida Jr.[1],

Karina A. Toledo[1], Osvaldo N. Oliveira Jr.[2], Pedro H. B. Aoki[1*]

[1]São Paulo State University (UNESP), School of Sciences, Humanities and Languages, Assis, SP, 19806-900, Brazil. *pedro.aoki@unesp.br

[2]São Carlos Institute of Physics, University of São Paulo (USP), CP 369, São Carlos, SP, 13566-590, Brazil.

Short statistical summary

Words: 6,680.0
Figures: 6
Tables: 1

Abstract

Metallic nanoparticles are promising agents for photothermal cancer therapy (PTT) owing to their photostability and efficient light-to-heat conversion, but their possible aggregation remains an issue. In this paper, we report on the photoinduced heating of gold shell-isolated nanoparticles (AuSHINs) in *in vitro* experiments to kill human oropharyngeal (HEp-2) and breast (BT-474 and MCF-7) carcinoma cells, with cell viability reducing below 50% with $2.2x10^{12}$ AuSHINs/mL and 6h of incubation. This toxicity to cancer cells is significantly higher than in previous works with gold nanoparticles. Considering the AuSHINs dimensions we hypothesize that cell uptake is not straightforward, and the mechanism of action involves accumulation on phospholipid membranes as the PTT target for photoinduced heating and subsequent generation of reactive oxygen species (ROS). Using Langmuir monolayers as simplified membrane models, we confirmed that AuSHINs have a larger effect on 1,2-dioleoyl-sn-glycero-3-phospho-L-serine (DOPS), believed to represent cancer cell membranes, than on 1,2-dioleoyl-sn-glycero-3-phosphocholine (DOPC) taken as representative of healthy eukaryotic cells. In particular, data from polarization-modulated infrared reflection absorption spectroscopy (PM-IRRAS) revealed an increased conformational order of DOPS tails due to the stronger adsorption of AuSHINs. Furthermore, light irradiation reduced the stability of AuSHINs containing DOPC and DOPS monolayers owing to oxidative reactions triggered by ROS upon photoinduced heating. Compared to DOPC, DOPS lost nearly twice as much material to the subphase, which is consistent with a higher rate of ROS formation in the vicinity of the DOPS monolayer.

1. Introduction

Light-based therapies are suitable to destroy malignant cells in less invasive clinical treatments,[1,2] as is the case of photothermal therapy (PTT)[3–7] for cervical (HeLa)[8], breast (SK-BR-3 and MCF-7),[9,10] oral squamous (HSC-3 and HOC-313)[11] and skin (A375)[12] carcinomas. PTT is based on the administration of a photothermal agent (PTA), which can increase the local temperature by tens of degrees upon light activation.[13–15] Indeed, cancer cells can be selectively destroyed since the tumor environment is more hypoxic, acidic and nutrient-deficient, which make them sensitive to higher temperatures.[9,16] Synthetic dyes have been employed as PTA owing to the high efficiency in converting the absorbed light into heat.[15,17] However, most of the dyes can be quickly photobleached, and therefore there is demand for efficient and stable PTAs. Nanostructured materials such as gold nanoparticles (AuNP) are photostable and absorb light from the UV-vis to NIR,[17,18] being attractive for PTT.[19]

In the AuNP light-excitation, the oscillating electric field of the irradiation leads to a coherent oscillation of free electrons in the conduction band,[20,21] giving rise to the so-called localized surface plasmon resonance (LSPR). The latter results in strong electromagnetic fields and enhances the scattering and absorption of light by the nanoparticles.[22–24] LSPR can be adjusted to be in full resonance with the excitation wavelength by tuning the size and shape of the AuNPs.[5,25,26] Spherical AuNPs with 10-40 nm diameter are considered non-toxic to healthy tissues[27,28] and are efficient in light-to-heat conversion.[9,16,29] However, AuNPs may destabilize, aggregate and lose thermal efficiency in high ionic strength media, which is a limitation for *in vitro* and *in vivo* assays.[30–32] Shell-isolated gold nanoparticles (AuSHINs) are surface modified AuNP with an ultrathin silica shell (2 – 4 nm), less amenable to aggregation, and should thus be considered for PTT.[33,34]

In this paper, we employ AuSHINs to demonstrate that photoinduced heating can kill different types of cancer cells in *in vitro* experiments. We also investigate the possible mechanisms of action, assuming that plasma membranes are important targets in PTT.[35,36] Membrane perturbation, cytoskeleton disordering, and protein denaturing[6,37,38] are known cellular effects induced by PTT, but the complexity of plasma membrane prevents the *in vivo* determination of such molecular mechanisms. Herein, we probe such interactions by representing the cell membranes with Langmuir monolayers[39–42] in order to obtain molecular-level information. We mimic the cell membranes of healthy eukaryotic cells and cancer cells by selecting two distinct types of phospholipids, namely 1,2-dioleoyl-sn-glycero-3-phosphocholine (DOPC) and 1,2-dioleoyl-sn-glycero-3-phospho-L-serine (DOPS). Phosphatidylserines are overexpressed on the outer leaflet of tumor membranes[43–45] while healthy cells are predominantly composed of phosphatidylcholines.[46,47] The mechanism of AuSHINs adsorption on the monolayers and effects of irradiation were evaluated using surface-pressure-area isotherms (π-A) and polarization-modulated infrared reflection absorption spectroscopy (PM-IRRAS).[48,49]

2. Experimental section

2.1. Materials

The 1,2-dioleoyl-sn-glycero-3-phosphocholine (DOPC) and 1,2-dioleoyl-sn-glycero-3-phospho-L-serine (DOPS) were purchased from Avanti Polar Lipids and their structures are presented in Figure 1a. Tetrachloroauric acid ($HAuCl_4.3H_2O$, 99.9%), sodium silicate solution (10.6% Na_2O and 26.5% SiO_2, d = 1.39 g/mL), sodium citrate ($C_6H_5Na_3O_7.2H_2O$, ≥ 99%), N-acetyl-L-cysteine (NAC, $HSCH_2CH(NHCOCH_3)CO_2H$, ≥ 99%), (3-aminopropyl) trimethoxysilane ($C_6H_{17}NO_3Si$, d = 97%) and chloroform were acquired from Sigma-Aldrich. The materials were used as received with no further purification. A Milli-Q system (Direct- Q® 3UV) was employed to produce ultrapure water (pH 5.8 and 18.2 MΩ.cm).

2.2. Synthesis and coating of gold nanoparticles

Gold nanoparticles (AuNPs) and gold shell-isolated nanoparticles (AuSHINs) were synthesized using the procedures established by Aroca et al.[50] and Li et al.[34], with slight modifications. AuNPs were prepared by adding 7.5 mL of sodium citrate at 38.8 mmol/L in 150 mL of a boiling $HAuCl_4$ solution at 0.5 mmol/L under heating and magnetic stirring. Heating and stirring were continued for 10 min after the solution becomes reddish-purple, which was subsequently stirred for more 15 min. The colloidal suspension was cooled to ca. 25ºC and stored for further characterization and coating. AuNPs with a silica shell were obtained by mixing 3 mL of APTMS solution at 1 mmol/L with 50 mL of AuNPs, under vigorous stirring for 10 min. 6 mL of 0.54 % sodium silicate aqueous solution (pH = 10) were then added and stirred for 3 min. The mixture was finally heated to 90 – 95°C for 3h. The characterization of AuNPs and AuSHINs was carried out by UV-Vis absorption spectroscopy (Agilent, Cary 60), transmission electron microscopy (JEOL JEM-1400) and zeta potential (Malvern Panalytical, model Zetasizer Nano S90).

A core size of 15.9 ± 1.5 nm and a SiO_2 shell thickness of 5.5 ± 1.0 nm were obtained, as shown in Figures 1b and SI1. The silica coating of AuNPs changes the refractive index of the nanoparticles and induce a red shift in the extinction spectra from 519 to 524 nm (Figure 1b).[32,50] In addition, changes in the zeta potential values, from – 58.4 mV to -31.9 mV, were also observed as a result of the silica shell.

2.3. In vitro studies

The human cell lines HEp-2 (oropharyngeal carcinoma; ref.0101), BT-474 (ductal breast carcinoma; ref. 0353) and MCF-7 (glandular breast carcinoma; ref. 0162) were provided by the Cell Bank from Rio de Janeiro (RJ - Brazil) and used in the *in vitro* experiments. The cells were cultured in T-75 flasks (ref. 3290; Corning Glass Works, Corning, NY, USA) within sterile environment under 5% CO_2 at 37 °C, following previous established protocols.[51,52] HEp-2, MCF-7 and BT-474 cells were then grown in 96-well plates for further incubation with either AuNPs or AuSHINs during 2h and 6h. Different concentrations of nanoparticles were added to the cells: $6.5x10^{12}$ of AuNPs/mL and $2.2x10^{12}$, $5.5x10^{12}$, and $2.2x10^{13}$ of AuSHINs/mL, respectively. The cells were irradiated for 1h using a green LED (BioLambda, 525 nm) with 118 J/cm^2 of irradiance and power of 32.8 mW/cm^2. The metabolism of the cell lines was measured via MTT assays [3-(4,5-7 dimethylthiazol-2-yl)-2,5-diphenyltetrazolium bromide] (ref. M2003; Sigma Aldrich), by removing the culture medium and rinsing the cells with PBS for subsequent incubation (ca. 50 min) with 0.5 g/L of MTT. The formazan crystals were solubilized in 50 $x10^{-6}$ L of dimethylsulfoxide and the absorbance was measured at 560 nm in a Multiskan™ FC Microplate Photometer.[53] Cells cultured without AuNPs or AuSHINs were considered 100% viable and used as cellular control (CC). The death control (DC) was obtained with the addition of $50x10^{-6}$ mol/L of hydrogen peroxide, while the light control (LC) with irradiation of the cell culture in the absence of AuNPs

or AuSHINs. AuNPs and AuSHINs experimental data were plotted with GraphPad Prim® 8 and evaluated by analysis of variance (one-unpaired multiple t test), following Bonferroni test ($P \leq 0.001$). All the tests were performed in triplicate.

2.4. Langmuir monolayers

DOPC and DOPS Langmuir monolayers were formed on ultrapure water and on a colloidal suspension of AuSHINs using a KSV-NIMA 2002 trough. The colloid concentration was estimated as $2.7x10^{12}$ AuSHINs/mL, following a previous protocol.[32] A platinum plate was used as Wilhelmy sensor to obtain the surface pressure (π), thus allowing isotherms versus mean molecular area (A) to be obtained. Chloroform solutions of phospholipids at 1 mmol/L were spread on the subphases, which were kept at 23 ^{o}C. The solvent was allowed to evaporate for 10 min before the symmetric compression of the barriers at a constant speed of 10 mm/min. All the experiments were performed at pH 5.8, with no need of further correction. No precautions were taken to prevent oxidation from reactive species of the environment[54] but we have ensured that the surface pressure at a given area per molecule was within ± 2 mN/m. Irradiation was carried out at 30 mN/m positioning the LED (530 nm / 50 W, BRIWAX FFG) source 20 cm above the monolayer interface, as indicated in Figure 1c. Changes in the mean molecular area of the monolayers were followed over 130 min. Polarization-modulated infrared reflection-absorption spectroscopy (PM-IRRAS, KSV PMI550) experiments were performed with an incidence angle of 81° and 8 cm^{-1} of resolution. The spectra were carried out for irradiated and non-irradiated DOPC and DOPS monolayers at 30 mN/m on AuSHINs subphases and ultrapure water. In the case of irradiated monolayers, the PM-IRRAS spectra were taken right after the irradiation period with the LED source. The spectral reproducibility was confirmed by repeating each experiment at least three times. Therefore, modifications in the band position and/or relative intensity are not related to

spectral dispersion, but rather to interactions with AuSHINs and due to irradiation of the lipid monolayers, on AuSHINs, with the green LED (530 nm).

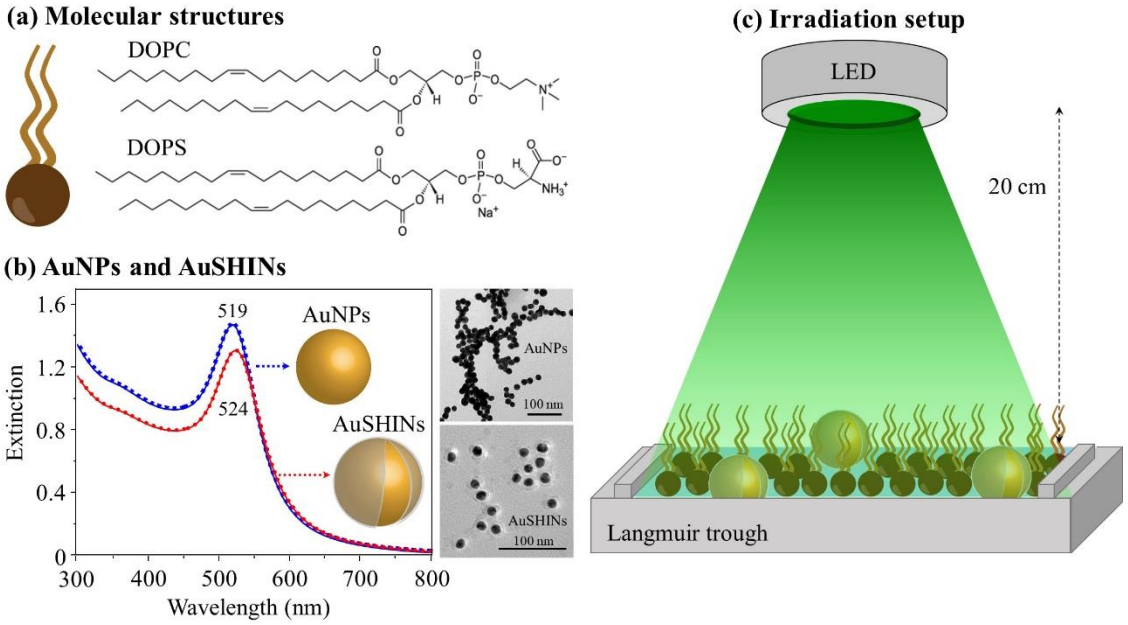

Figure 1. (a) DOPC and DOPS molecular structures. (b) Extinction spectra and TEM images of AuNPs and AuSHINs. (c) Schematic representation of lipid monolayers interacting with AuSHINs under irradiation.

3. Results and Discussion

3.1. Toxic and phototoxic effects of AuSHINs on cancer cells

The toxic and phototoxic effects of AuSHINs were evaluated in cells derived from oropharyngeal (HEp-2), glandular (MCF-7) and ductal (BT-474) breast carcinomas using MTT assays, whose results are shown in Figures 2a-f. Colloidal suspensions at $2.2x10^{12}$, $5.5x10^{12}$, and $2.2x10^{13}$ AuSHINs/mL were incubated in the cells for 2h and 6h in the dark and then irradiated (525 nm) for 1h. Cell viability was not affected during the 2h of incubation in the dark (Figures 2a, 2c and 2e), except for a slight increase in the metabolism of MCF-7 (Figure 2c) and BT-474 (Figure 2e) cells for concentrations above $5.5x10^{12}$ AuSHINs/mL, which might be indicative of early apoptosis.[55] AuSHINs presented only a mild toxicity for MCF-7 and BT-474 above $2.2x10^{13}$ AuSHINs/mL incubated for 6h in the dark, as shown in Figures 2d and 2f. On the other hand, the cell culture is significantly affected by irradiation and viability is reduced below 50% (CC_{50}) at $5.5x10^{12}$ AuSHINs/mL for HEp-2 and $2.2x10^{12}$ AuSHINs/mL for MCF-7 and BT-474 cells with 2h of incubation. Considering 6h of incubation time, the viability of all the cell lines is reduced below 50% starting with $2.2x10^{12}$ AuSHINs/mL. The decrease of the viable population with incubation time suggests an increase in the incorporated AuSHINs by the cells that further allows greater efficiency in reducing cell viability, similarly to the observed for photosensitizers.[56] Control experiments with AuNPs were less effective in reducing cell viability under irradiation owing to the aggregation of the nanostructures triggered by the ionic strength of the medium.[57] Compared to the available data in the literature, the CC_{50} achieved here for MCF-7 with 2h of incubation was obtained with ca. half of the light dose required in similar works using AuNP coated with polyethyleneglycol (PEG),[9] highlighting the high photothermal efficiency of AuSHINs. The light-induced increase in temperature of more than 16 ^{o}C (Figure SI2) denatures proteins and may open pores in the plasma membrane,[9,58] which are likely

to be the origins of the phototoxicity observed. Additionally, subsidiary experiments using the antioxidant N-acetyl-L-cystein (NAC) revealed an increase in cell viability owing to the suppression of ROS available in the medium (Figure SI3).[59] The latter not only confirms the generation of ROS during local heating but also suggests that oxidative reactions play a role in the cellular phototoxicity,[6,37,38] which is consistent with the data on Langmuir monolayers to be presented in the next section.

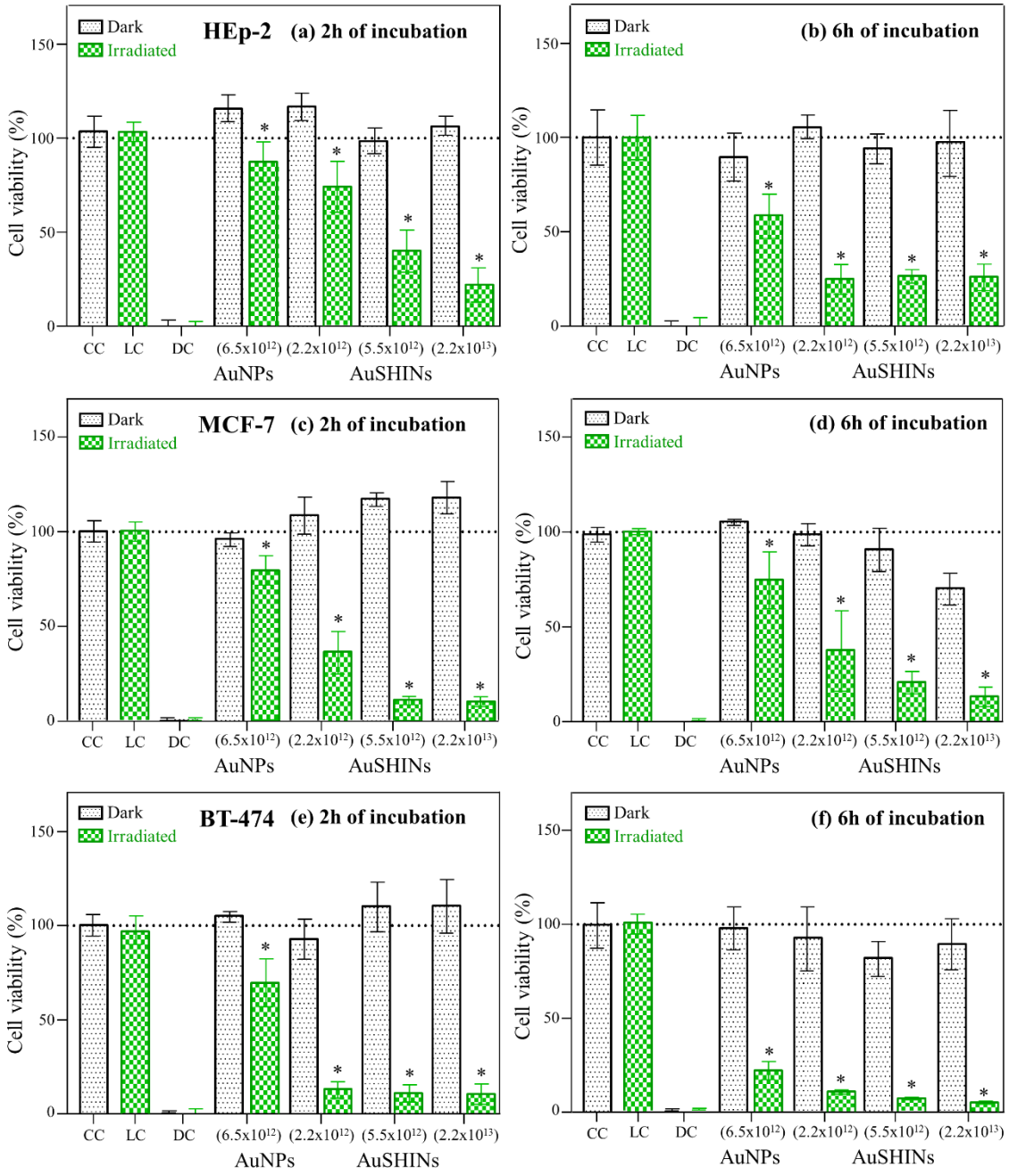

Figure 2. Toxic (dark) and phototoxic (irradiated) effects of $2.2x10^{12}$, $5.5x10^{12}$, and $2.2x10^{13}$ AuSHINs/mL on HEp-2, MCF-7 and BT-474 cells measured by MTT after 2h

(a, c, e) and 6h (b, d, f) of incubation, respectively. Assays with $6.5x10^{12}$ AuNPs/mL were used as controls. *P<0.001 (multiple t tests, Bonferroni), in relation to the non-irradiated population. CC correspond to the cellular control; DC is the death control and LC is the light control.

3.2 *AuSHINs incorporation into DOPC and DOPS Langmuir films*

The π-A isotherms of DOPC and DOPS monolayers on ultrapure water and AuSHINs are shown in Figures 3a and 3b, respectively. Subsidiary experiments have shown that AuSHINs cannot form Langmuir monolayers. The isotherms indicate that AuSHINs expand the DOPC and DOPS monolayers, suggesting their incorporation. Expansion is slightly larger for DOPS, which may seem surprising since AuSHINs are also negatively charged with a zeta potential of -39.1 mV. However, even though ionic forces are prominent in the interaction between nanoparticles and cell membrane models, other factors such as morphology, size, surface modification[35,41,60] and secondary interactions are also relevant. Indeed, Torrano et al.[60] and Lins et al.[41] suggested that AuNPs were incorporated into DPPC monolayers due to attractive interactions with the choline group of polar heads. Since DOPC and DPPC share phosphatidyl moieties, interactions of the same nature should govern the adsorption of AuSHINs onto DOPC monolayers. Despite the net negative charge of DOPS,[61] their cationic NH_3^+ group may be involved in electrostatic interactions with AuSHINs, as will be demonstrated with PM-IRRAS results later on in this paper. Moreover, sodium counter ions (Na^+) surrounding the DOPS molecules could minimize the repulsion effect with the AuSHINs, allowing AuSHINs to be incorporated via van der Walls interactions. This additional attractive interaction, of secondary nature, may help to explain the larger expansion for DOPS monolayers.

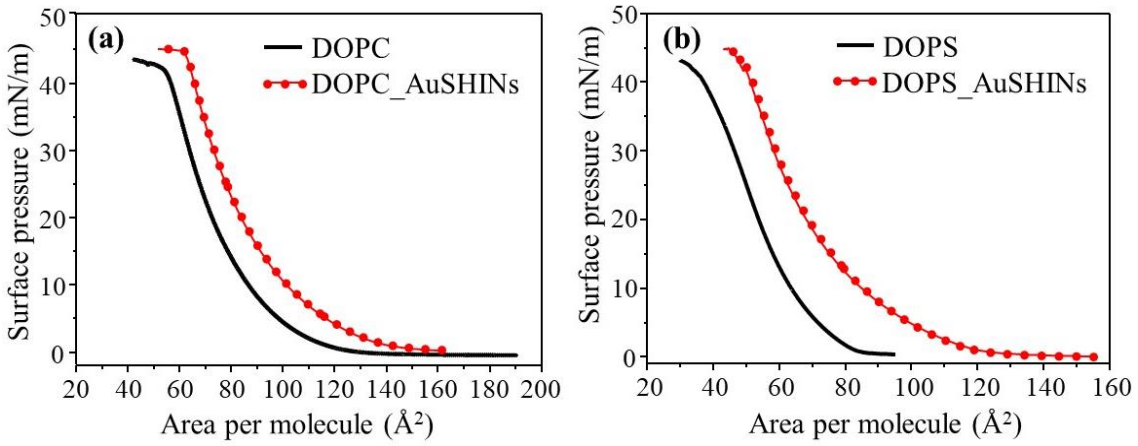

Figure 3. π-A isotherms of (a) DOPC and (b) DOPS on ultrapure water and AuSHINs subphases.

Molecular-level interactions between AuSHINs and the monolayers were assessed here with PM-IRRAS, whose spectra for DOPC on AuSHINs and ultrapure water subphases are given in Figure 4a. Table 1 provides the assignments of the bands along with the displacements induced by AuSHINs insertion and by irradiation. The incorporation of AuSHINs into DOPC monolayers affects the bands of the head groups and chains. For instance, the antisymmetric stretching of $CN^{+}(CH_3)_3$ shifted from 950 to 958 cm^{-1} and had an increase in intensity, which suggests a reorientation of the choline group owing to the attractive electrostatic interactions with AuSHINs. The $\nu(C\text{-}O\text{-}PO_2^{-})$ at 1032 cm^{-1} and $\nu(PO_2^{-})$ at 1065 cm^{-1} shifted to 1021cm^{-1} and 1052 cm^{-1}, with inversion in the relative intensity, indicating hydration of phosphate groups.[62] The band due to $\nu_{as}PO_2^{-}$ at 1223 cm^{-1} splits to 1190 and 1216 cm^{-1}, which is evidence of H-bonded PO_2.[63] The band at 1565 cm^{-1} corresponds to vibrational modes of AuSHINs (Figure SI4), confirming their incorporation into the monolayer. Another evidence of AuSHINs incorporation is the increase of $\delta(H_2O)$ at 1678 cm^{-1}.[35] The 1600-1700 cm^{-1} region is characteristic of the water interface reflectivity.[40,42,64] The higher $\delta(H_2O)$ intensity, the larger the regions on which the water interface is not covered with the monolayer,[65] which is consistent with AuSHINs incorporation. In addition, $\nu(C{=}O)$ at 1732 cm^{-1} shifted

to 1751 cm^{-1} and had the intensity decreased, similarly to the results by Caseli et al.[35] for DPPC monolayers interacting with AuNPs.

AuSHINs adsorption also affected the bands assigned to the aliphatic chains. The $\nu_s(CH_2)$ and $\nu_{as}(CH_2)$ bands at 2848 and 2934 cm^{-1} shifted to 2845 and 2915 cm^{-1}, respectively. The $\nu_s(CH_2)$ and $\nu_{as}(CH_2)$ intensity ratio (I_s/I_{as})[66] was not altered, which could indicate that the conformational order of the chains was not affected by AuSHINs.[49] However, the shift of $\nu_{as}(CH_2)$ band to lower wavenumber suggests that the alkyl chains undergo to an all-*trans* conformation, which is a more ordered structure.[67–69] The $\nu_s(CH_3)$ band at 2880 cm^{-1} disappears owing to the reorientation of the group upon AuSHINs interaction. A mechanism of interaction is proposed in Figure 4b where AuSHINs are inserted into the DOPC monolayer nearby the choline, phosphate and carbonyl groups. It is likely that the interaction with AuSHINs may have changed the dipole orientation of the zwitterionic headgroup, which is oriented almost parallel to the air/water interface on neat DOPC monolayers (Figure 4b - left panel).[70–72]

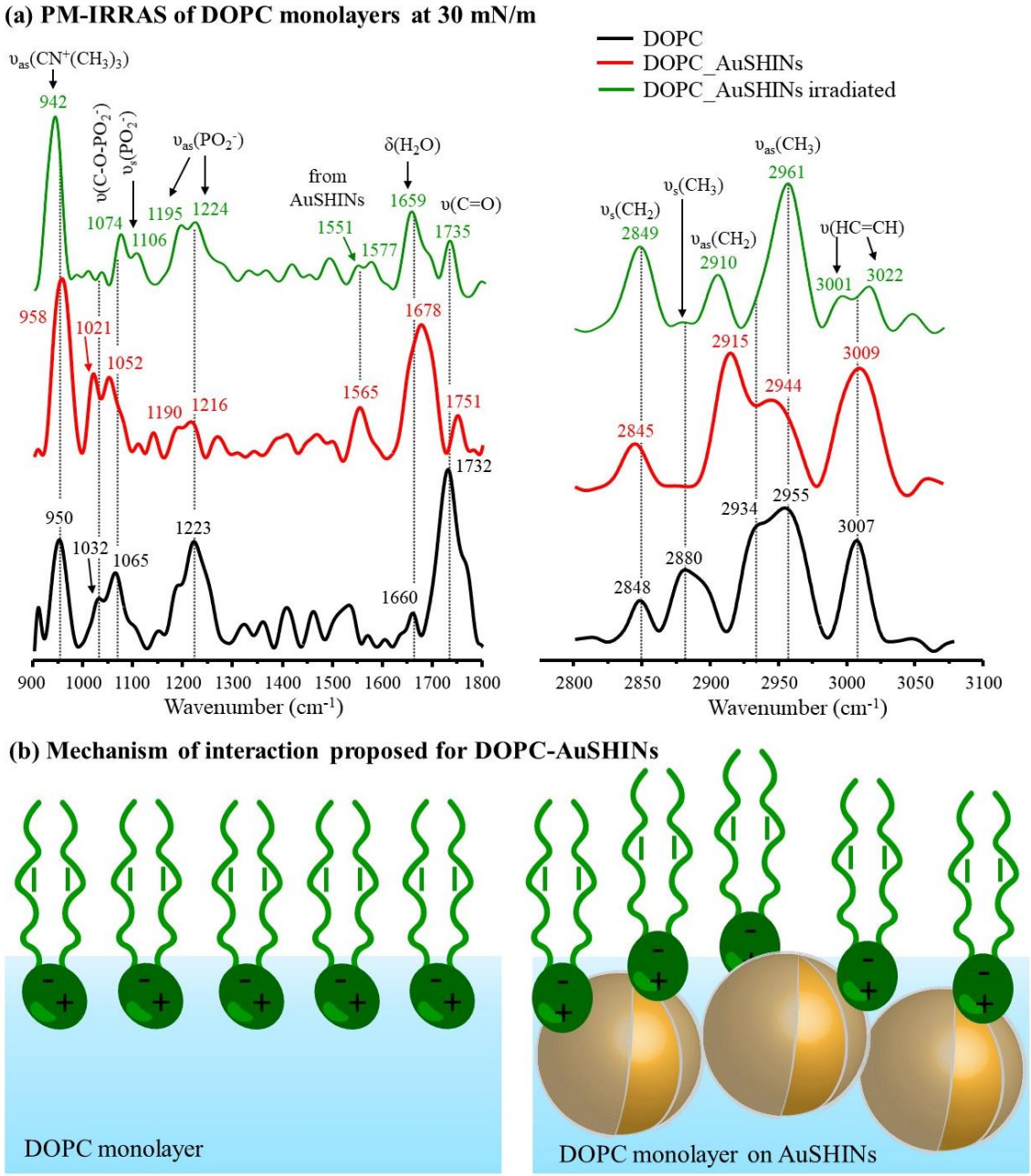

Figure 4. (a) PM-IRRAS spectra of DOPC monolayers on AuSHINs and ultrapure water, before and after irradiation. (b) DOPC-AuSHIN mechanism of interaction. The left panel represents the DOPC monolayer at the air/water interface while the right panel shows how DOPC monolayer interacts with AuSHINs subphase.

The PM-IRRAS spectra for DOPS on AuSHINs and ultrapure water subphases are given in Figure 5a. The NH_3^+ rocking and C-N stretching mode shifted from 922 to 949 cm^{-1},[73] confirming the attractive electrostatic interactions between the ammonium group ($-NH_3^+$) of DOPS and the negatively charged AuSHINs. The incorporation of AuSHINs also affects the phosphate group as follows: (i) $\nu(C\text{-}O\text{-}PO_2^-)$ shifted from 1049

to 1066 cm^{-1} and had the intensity increased; (ii) $\nu_s(PO_2^-)$ at 1139 cm^{-1} displaced to 1128 cm^{-1}, indicating hydration of the phosphate group;[62] and (iii) $\nu_{as}(PO_2^-)$ at 1211 cm^{-1} shifted to 1220 cm^{-1} and enhanced the intensity. The latter indicates that AuSHINs induce H-bonds between PO_2^- groups in the monolayer.[63] The $\nu_{as}(COO^-)$ band of serine[62,74,75] at 1556 cm^{-1} displaced to 1580 cm^{-1}, which may also be related to electrostatic interactions with AuSHINs. The bending mode of water (δH_2O) at 1659 cm^{-1} shifted to 1687 cm^{-1} and had the intensity increased, indicating that the air/water interface is not entirely covered by the monolayer owing to AuSHINs incorporation.[65] In addition, ν(C=O) at 1733 cm^{-1} [63] shifted to 1751 cm^{-1} and had the intensity enhanced.

As for the hydrophobic tails, the $\nu_s(CH_2)$ and $\nu_{as}(CH_2)$ intensity ratio (I_s/I_{as}) reduced from 1.22 to 0.37 upon AuSHINs incorporation, indicating an increased conformational order of the chains.[49] The CH_3 symmetric and antisymmetric stretching bands at 2895 cm^{-1} and 2952 cm^{-1} had the intensity significantly decreased, probably because of the increased order and packing of the chains. In addition, ν(HC=CH) at 3000 cm^{-1} displaced to 2989 cm^{-1} upon AuSHINs incorporation. Overall, a deeper penetration of AuSHINs into DOPS monolayers may have led to more meaningful modifications in the hydrocarbon chains, in contrast to what occurred for DOPC monolayers. DOPS is a negatively charged phospholipid which tends to establish intermolecular attractions between the carboxylic and ammonium groups.[76] The headgroups are therefore oriented closer to each other with highly disordered tails, as depicted in Figure 5b (left panel). The incorporation of AuSHINs disrupts these intermolecular attractions inducing chain order, as shown in Figure 5b (right panel).

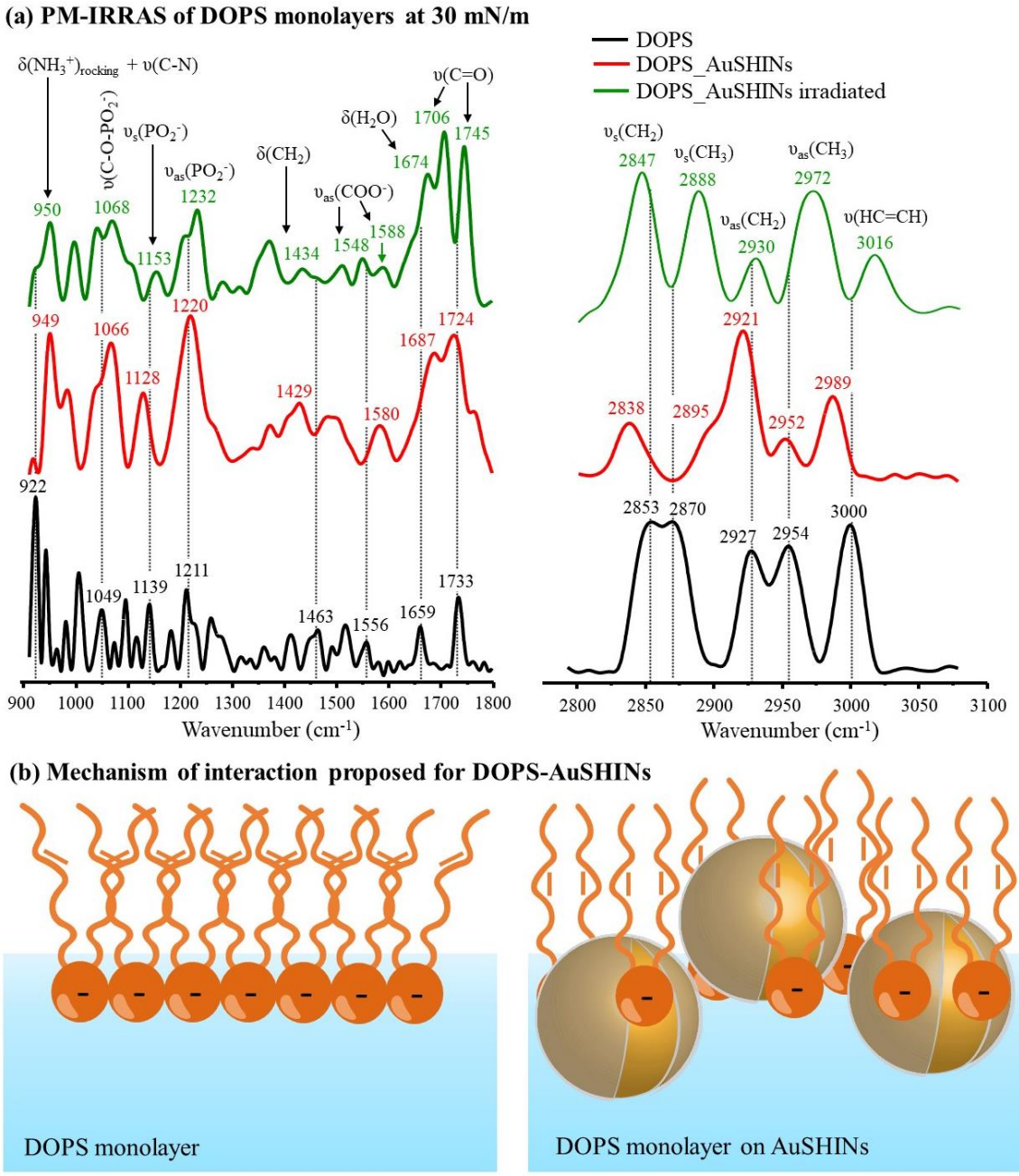

Figure 5. (a) PM-IRRAS spectra of DOPS monolayers on AuSHINs and ultrapure water, before and after irradiation. (b) DOPS-AuSHIN mechanism of interaction. The left panel shows the DOPS monolayer at the air/water interface while the right panel indicates how the DOPS monolayer interacts with AuSHINs.

Table 1. Assignments of the main bands for neat DOPC and DOPS monolayers and shifts induced upon AuSHINs interaction and irradiation.

DOPC (cm^{-1})			DOPS (cm^{-1})			Assignments
water	**AuSHINs**	**AuSHINs + light**	**water**	**AuSHINs**	**AuSHINs +light**	
-	-	-	922	949	950	$\delta(NH_3^+)_{rocking}$ + υ(C-N)
950	958	942	-	-	-	$\upsilon_{as}(CN^+(CH_3)_3)$
1032	1021	1074	1049	1066	1068	υ(C-O-PO_2^-)
1065	1052	1106	1139	1128	1153	$\upsilon_s(PO_2^-)$
1223	1190 and 1216	1195 and 1224	1211	1220	1232	$\upsilon_{as}(PO_2^-)$
-	-	-	1463	1429	1434	$\delta(CH_2)$
-	-	-	1556	1580	1548 and 1588	$\upsilon_{as}(COO^-)$
-	1565	1551 and 1577	-	-	-	AuSHINs
1660	1678	1659	1659	1687	1674	$\delta(H_2O)$
1732	1751	1735	1733	1724	1706 and 1745	υ(C=O)
2848	2845	2849	2853	2838	2847	$\upsilon_s(CH_2)$
2880	-	-	2870	2895	2888	$\upsilon_s(CH_3)$
2934	2915	2910	2927	2921	2930	$\upsilon_{as}(CH_2)$
2955	2944	2961	2954	2952	2972	$\upsilon_{as}(CH_3)$
3007	3009	3001 and 3022	3000	2989	3016	υ(HC=CH)

3.3. AuSHINs photoactivation and photo-induced modifications in the lipid monolayers

Photo-induced modifications in DOPC and DOPS monolayers on AuSHINs subphase were probed at 30 mN/m using green light (530 nm) irradiation. Figure 6 displays the time dependence for the surface area of irradiated and nonirradiated DOPC and DOPS monolayers. Subsidiary experiments have shown that irradiation of DOPC and DOPS on water subphase did not produce any significant modification. A material loss to the subphase explains the area decrease for all the nonirradiated monolayers, as a result of uncontrolled oxidation from reactive species of the environment.[77] The slope of area decrease for DOPC and DOPS is increased upon irradiation, suggesting an increased material loss, similar to the UV damage[78] and ozone oxidation.[79,80]

AuSHINs can sustain LSPR under irradiation[15] and the free electron oscillation can increase the local temperature by up to 16 ^{o}C, as demonstrated in subsidiary experiments (Figure SI2). The local increase in temperature enhances the level of reactive oxygen species (ROS)[6,81] (Figure S3) that can further oxidize the unsaturated chains[82–84] of the lipid membranes. The main results of these oxidative reactions may include: (i) increased water solubility of the lipids; (ii) restricted chain fluidity owing to hydrogen bonds with the surrounding water;[85] and (iii) chain cleavage and generation of water soluble aldehydes or alcohols.[86] The latter might be the origin of the attenuated material loss observed for DOPC and DOPS monolayers. The nearly 16% of area decrease in DOPS is larger than the ca. 8% of decrease for DOPC, which can be related to the stronger adsorption of AuSHINs onto DOPS monolayers. The larger amount of adsorbed AuSHINs induces a higher rate of ROS generation in the vicinity of the DOPS monolayer, favoring the oxidative reactions. Therefore, stronger interactions between AuSHINs and phosphatidylserines on tumor cells must play a role in the photothermal efficiency, favoring not only localized heating but also the oxidative stress that further induce cellular death. Combined with the increased sensitivity to hyperthermia, cancer cells can thus be selectively destroyed as reported in the literature.[9,16]

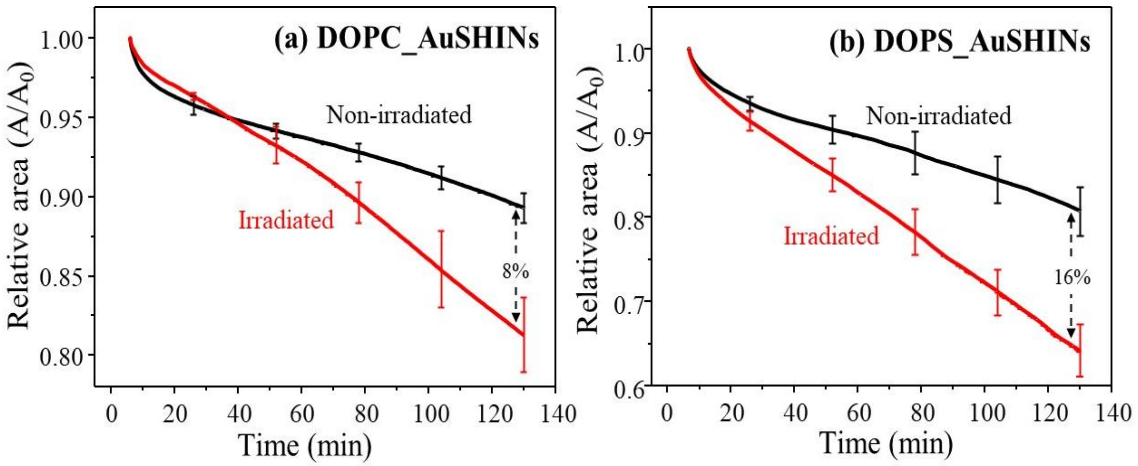

Figure 6. Relative area (A/A_0) evolution recorded at 30 mN/m for irradiated and non-irradiated (a) DOPC and (b) DOPS monolayers on AuSHINs subphase. A_0 was extrapolated from 30 mN/m down to zero pressure.

Irradiation affected head groups and tails of DOPC monolayers on AuSHINs, as shown by the PM-IRRAS spectrum of Figure 4a. The $\nu_{as}(CN^{+}(CH_3)_3)$, $\upsilon(C\text{-}O\text{-}PO_2^{-})$, $\nu_s(PO_2^{-})$ and $\nu_{as}(PO_2^{-})$ displaced from 958, 1021, 1052 and 1190 and 1216 cm^{-1} to 942, 1074, 1106, and 1195 and 1224 cm^{-1}, respectively. Changes in the vibrational modes of the phosphates indicate that H-bonding with water molecules is affected by irradiation.[63] Modifications in the carbonyl ester group are also observed, with a shift from 1751 to 1735 cm^{-1}. As for the tails (i) the $\nu_s(CH_2)$ and $\nu_{as}(CH_2)$ intensity ratio (I_s/I_{as}) increased from 0.32 to 1.6 and (ii) the intensity of $\upsilon(HC=CH)$ at 3009 cm^{-1} decreased, with a band split to 3001 and 3022 cm^{-1}. The conformational order of the alkyl chains is therefore reduced and the effects over the unsaturation moiety are consistent with the oxidative reactions triggered by ROS.

Similar effects were observed for irradiated DOPS monolayers in Figure 5a. The $\upsilon_s(PO_2^{-})$ and $\upsilon_{as}(PO_2^{-})$ were shifted from 1128 and 1220 cm^{-1} to 1153 and 1232 cm^{-1}, suggesting dehydration of the phosphate group.[62] $\upsilon_{as}(COO^{-})$ at 1580 displaced to 1588 cm^{-1} and a new band appears at 1548 cm^{-1} assigned to AuSHINs (Figure SI4). Furthermore, the nonhydrated $\upsilon(C=O)$ shifted from 1724 to 1745 cm^{-1} and the hydrated $\upsilon(C=O)$ at 1706 cm^{-1} had an increase in intensity. It is known that the shape and position of the carbonyl ester group depend on the hydration of the polar groups and on the polarity of the medium.[87] Upon irradiation, changes in the carbonyl solvation[88] might lead to hydration. Regarding the tails, the $\nu_s(CH_2)$ and $\nu_{as}(CH_2)$ intensity ratio(I_s/I_{as}) enhanced from 0.37 to 2.98, suggesting a decreased conformational chain order,[49] similarly to what was observed for DOPC. In addition, the displacement of the $\nu_{as}(CH_2)$ band to higher wavenumbers (from 2921 to 2930 cm^{-1}) indicates an increase in the *gauche*/*trans*

conformer ratio, which also suggest a more disordered structure of the alkyl tails.[67–69] υ(HC=CH) shifted from 2989 to 3016 cm^{-1}. Although the surface pressure experiments indicated an increased loss of material to the subphase, one might infer that the presence of υ(HC=CH) band on both DOPC and DOPS irradiated monolayers would not agree with the chain cleavage as the outcome of the oxidative reactions. However, it is likely that the by-products of the cleavage are expelled from the interface, leaving in the monolayers solely the uncleavage lipids to be probed.

4. Conclusion

Gold shell-isolated nanoparticles (AuSHINs) were successfully applied as photothermal agents in *in vitro* experiments with oropharyngeal (HEp-2) and breast (BT-474 and MCF-7) carcinoma cells, whose population was significantly reduced below 50% with the photoactivation of $2.2x10^{12}$ AuSHINs/mL incubated for 6h. This efficiency was correlated with the adsorption mechanism of AuSHINs on cell membranes, mimicked here by Langmuir monolayers of DOPC and DOPS as model systems of healthy and tumor cell membranes, respectively. π-A isotherms and PM-IRRAS have shown that the negatively charged AuSHINs adsorbed on both DOPC and DOPS monolayers mainly by attractive electrostatic interactions with the cationic choline and ammonium head groups, respectively. A larger expansion was observed for DOPS monolayer owing to the stronger adsorption that resulted in an increased conformational order of the chains. Under irradiation, both DOPC and DOPS monolayers became more unstable and increased the rate of the surface area decrease in ca. 8% and 16%, respectively. The reactive oxygen species (ROS) generated by local heating induces oxidative reactions that end up in the cleavage of chains, leading to the attenuated loss of material and membrane damage. The stronger AuSHINs adsorption on DOPS monolayers generated a higher amount of ROS in the vicinity of the monolayers, which is the origin of the higher rate of material loss upon irradiation. Together, these results help to understand the underlying mechanism behind the photothermal cancer therapy, which is relevant for applications.

Acknowledgments

This work was supported by São Paulo Research Foundation (FAPESP; 2018/14692-5, 2018/16713-0, 2013/14262-7, 2018/22214-6), INEO and National Council for Scientific and Technological Development (CNPq; Universal 403713/2016-1). We thank the technical assistance of Ana Claudia de Godoy Curro from IQSC- USP with the TEM images.

CONFLICTS OF INTEREST

There are no conflicts to declare.

References

[1] S. Ye, J. Rao, S. Qiu, J. Zhao, H. He, Z. Yan, T. Yang, Y. Deng, H. Ke, H. Yang, Y. Zhao, Z. Guo, H. Chen, Rational Design of Conjugated Photosensitizers with Controllable Photoconversion for Dually Cooperative Phototherapy, Adv. Mater. (2018). https://doi.org/10.1002/adma.201801216.

[2] X. Yan, H. Hu, J. Lin, A.J. Jin, G. Niu, S. Zhang, P. Huang, B. Shen, X. Chen, Optical and photoacoustic dual-modality imaging guided synergistic photodynamic/photothermal therapies, Nanoscale. (2015). https://doi.org/10.1039/c4nr06868h.

[3] Y. Liu, P. Bhattarai, Z. Dai, X. Chen, Photothermal therapy and photoacoustic imaging: Via nanotheranostics in fighting cancer, Chem. Soc. Rev. (2019). https://doi.org/10.1039/c8cs00618k.

[4] L. Zou, H. Wang, B. He, L. Zeng, T. Tan, H. Cao, X. He, Z. Zhang, S. Guo, Y. Li, Current approaches of photothermal therapy in treating cancer metastasis with nanotherapeutics, Theranostics. 6 (2016) 762–772. https://doi.org/10.7150/thno.14988.

[5] A. Amendoeira, L.R. García, A.R. Fernandes, P. V. Baptista, Light Irradiation of Gold Nanoparticles Toward Advanced Cancer Therapeutics, Adv. Ther. 3 (2020) 1900153. https://doi.org/10.1002/adtp.201900153.

[6] X. Hou, Y. Tao, Y. Pang, X. Li, G. Jiang, Y. Liu, Nanoparticle-based photothermal and photodynamic immunotherapy for tumor treatment, Int. J. Cancer. (2018). https://doi.org/10.1002/ijc.31717.

[7] M. D'Acunto, Detection of intracellular gold nanoparticles: An overview, Materials (Basel). (2018). https://doi.org/10.3390/ma11060882.

[8] B.D. Chithrani, A.A. Ghazani, W.C.W. Chan, Determining the size and shape dependence of gold nanoparticle uptake into mammalian cells, Nano Lett. (2006). https://doi.org/10.1021/nl052396o.

[9] R. Mendes, P. Pedrosa, J.C. Lima, A.R. Fernandes, P. V. Baptista, Photothermal enhancement of chemotherapy in breast cancer by visible irradiation of Gold Nanoparticles, Sci. Rep. 7 (2017). https://doi.org/10.1038/s41598-017-11491-8.

[10] W. Jiang, B.Y.S. Kim, J.T. Rutka, W.C.W. Chan, Nanoparticle-mediated cellular response is size-dependent, Nat. Nanotechnol. (2008). https://doi.org/10.1038/nnano.2008.30.

[11] I.H. El-Sayed, X. Huang, M.A. El-Sayed, Selective laser photo-thermal therapy of epithelial carcinoma using anti-EGFR antibody conjugated gold nanoparticles, Cancer Lett. 239 (2006) 129–135. https://doi.org/10.1016/j.canlet.2005.07.035.

[12] S. Nouri, E. Mohammadi, B. Mehravi, F. Majidi, K. Ashtari, A. Neshasteh-Riz, S. Einali, NIR triggered glycosylated gold nanoshell as a photothermal agent on melanoma cancer cells, Artif. Cells, Nanomedicine Biotechnol. (2019). https://doi.org/10.1080/21691401.2019.1593187.

[13] P. Wust, B. Hildebrandt, G. Sreenivasa, B. Rau, J. Gellermann, H. Riess, R. Felix, P. Schlag, Hyperthermia in combined treatment of cancer, Lancet Oncol. (2002). https://doi.org/10.1016/S1470-2045(02)00818-5.

[14] R.W.Y. Habash, R. Bansal, D. Krewski, H.T. Alhafid, Thermal therapy, Part 2: Hyperthermia techniques, Crit. Rev. Biomed. Eng. (2006). https://doi.org/10.1615/CritRevBiomedEng.v34.i6.30.

[15] N.S. Abadeer, C.J. Murphy, Recent Progress in Cancer Thermal Therapy Using Gold Nanoparticles, J. Phys. Chem. C. (2016). https://doi.org/10.1021/acs.jpcc.5b11232.

[16] R.M. Cabral, P. V. Baptista, The chemistry and biology of gold nanoparticle-

mediated phototermal therapy promises and challenges, Nano Life. 03 (2013) 1330001. https://doi.org/10.1142/S179398441330001X.
[17] X. Huang, P.K. Jain, I.H. El-Sayed, M.A. El-Sayed, Plasmonic photothermal therapy (PPTT) using gold nanoparticles, Lasers Med. Sci. (2008). https://doi.org/10.1007/s10103-007-0470-x.
[18] J. Yguerabide, E.E. Yguerabide, Light-scattering submicroscopic particles as highly fluorescent analogs and their use as tracer labels in clinical and biological applications II. Experimental characterization, Anal. Biochem. (1998). https://doi.org/10.1006/abio.1998.2760.
[19] M.R.K. Ali, Y. Wu, M.A. El-Sayed, Gold-Nanoparticle-Assisted Plasmonic Photothermal Therapy Advances Toward Clinical Application, J. Phys. Chem. C. 123 (2019) 15375–15393. https://doi.org/10.1021/acs.jpcc.9b01961.
[20] G. Mie, Beiträge zur Optik trüber Medien, speziell kolloidaler Metallösungen, Ann. Phys. 330 (1908) 377–445. https://doi.org/10.1002/andp.19083300302.
[21] H.S. Kim, D.Y. Lee, Photothermal therapy with gold nanoparticles as an anticancer medication, J. Pharm. Investig. (2017). https://doi.org/10.1007/s40005-016-0292-6.
[22] J. Beik, M. Khateri, Z. Khosravi, S.K. Kamrava, S. Kooranifar, H. Ghaznavi, A. Shakeri-Zadeh, Gold nanoparticles in combinatorial cancer therapy strategies, Coord. Chem. Rev. (2019). https://doi.org/10.1016/j.ccr.2019.02.025.
[23] S. Akhter, M.Z. Ahmad, F.J. Ahmad, G. Storm, R.J. Kok, Gold nanoparticles in theranostic oncology: Current state-of-the-art, Expert Opin. Drug Deliv. (2012). https://doi.org/10.1517/17425247.2012.716824.
[24] R Aroca, Surface-Enhanced Vibrational Spectroscopy, John Wiley & Sons Ltd: Chichester ed: Toronto, 2006.
[25] H. Sharma, P.K. Mishra, S. Talegaonkar, B. Vaidya, Metal nanoparticles: A theranostic nanotool against cancer, Drug Discov. Today. 20 (2015) 1143–1151. https://doi.org/10.1016/j.drudis.2015.05.009.
[26] X. Huang, M.A. El-Sayed, Gold nanoparticles: Optical properties and implementations in cancer diagnosis and photothermal therapy, J. Adv. Res. 1 (2010) 13–28. https://doi.org/10.1016/j.jare.2010.02.002.
[27] J. Conde, M. Larguinho, A. Cordeiro, L.R. Raposo, P.M. Costa, S. Santos, M.S. Diniz, A.R. Fernandes, P. V. Baptista, Gold-nanobeacons for gene therapy: Evaluation of genotoxicity, cell toxicity and proteome profiling analysis, Nanotoxicology. 8 (2014) 521–532. https://doi.org/10.3109/17435390.2013.802821.
[28] P. Baptista, J. Conde, J. Rosa, P. Baptista, Gold-Nanobeacons as a theranostic system for the detection and inhibition of specific genes, Protoc. Exch. (2013). https://doi.org/10.1038/protex.2013.088.
[29] Z. Qin, Y. Wang, J. Randrianalisoa, V. Raeesi, W.C.W. Chan, W. Lipinski, J.C. Bischof, Quantitative comparison of photothermal heat generation between gold nanospheres and nanorods, Sci. Rep. 6 (2016). https://doi.org/10.1038/srep29836.
[30] J.-F. Li, C.-Y. Li, R.F. Aroca, Plasmon-enhanced fluorescence spectroscopy, Chem. Soc. Rev. 46 (2017) 3962–3979. https://doi.org/10.1039/C7CS00169J.
[31] S.A. Camacho, R.G. Sobral-Filho, P.H.B. Aoki, C.J.L. Constantino, A.G. Brolo, Zika Immunoassay Based on Surface-Enhanced Raman Scattering Nanoprobes, ACS Sensors. 3 (2018) 587–594. https://doi.org/10.1021/acssensors.7b00639.
[32] S.A. Camacho, R.G. Sobral-Filho, P.H.B. Aoki, C.J.L. Constantino, A.G. Brolo, Immunoassay quantification using surface-enhanced fluorescence (SEF) tags, Analyst. 142 (2017) 2717–2724. https://doi.org/10.1039/C7AN00639J.
[33] J.F. Li, Y.F. Huang, Y. Ding, Z.L. Yang, S.B. Li, X.S. Zhou, F.R. Fan, W. Zhang,

Z.Y. Zhou, D.Y. Wu, B. Ren, Z.L. Wang, Z.Q. Tian, Shell-isolated nanoparticle-enhanced Raman spectroscopy, Nature. 464 (2010) 392–395. https://doi.org/10.1038/nature08907.

[34] J.F. Li, X.D. Tian, S.B. Li, J.R. Anema, Z.L. Yang, Y. Ding, Y.F. Wu, Y.M. Zeng, Q.Z. Chen, B. Ren, Z.L. Wang, Z.Q. Tian, Surface analysis using shell-isolated nanoparticle-enhanced Raman spectroscopy., Nat. Protoc. 8 (2013) 52–65. https://doi.org/10.1038/nprot.2012.141.

[35] R.L.C.G. da Silva, H.F.O. da Silva, L.H. da Silva Gasparotto, L. Caseli, Lipopolysaccharides and peptidoglycans modulating the interaction of Au naparticles with cell membranes models at the air-water interface, Biophys. Chem. 238 (2018) 22–29. https://doi.org/10.1016/j.bpc.2018.04.007.

[36] R.L. Cruz Gomes da Silva, H.F. Oliveira da Silva, L.H. da Silva Gasparotto, L. Caseli, How the interaction of PVP-stabilized Ag nanoparticles with models of cellular membranes at the air-water interface is modulated by the monolayer composition, J. Colloid Interface Sci. 512 (2018) 792–800. https://doi.org/10.1016/j.jcis.2017.10.091.

[37] B. Hildebrandt, P. Wust, O. Ahlers, A. Dieing, G. Sreenivasa, T. Kerner, R. Felix, H. Riess, The cellular and molecular basis of hyperthermia, Crit. Rev. Oncol. Hematol. (2002). https://doi.org/10.1016/S1040-8428(01)00179-2.

[38] J.R. Lepock, Cellular effects of hyperthermia: Relevance to the minimum dose for thermal damage, in: Int. J. Hyperth., 2003. https://doi.org/10.1080/0265673031000065042.

[39] G.B. Soriano, R. da Silva Oliveira, F.F. Camilo, L. Caseli, Interaction of non-aqueous dispersions of silver nanoparticles with cellular membrane models, J. Colloid Interface Sci. 496 (2017) 111–117. https://doi.org/10.1016/j.jcis.2017.02.017.

[40] P.H.B. Aoki, L.F.C. Morato, F.J. Pavinatto, T.M. Nobre, C.J.L. Constantino, O.N. Oliveira, Molecular-Level Modifications Induced by Photo-Oxidation of Lipid Monolayers Interacting with Erythrosin, Langmuir. (2016). https://doi.org/10.1021/acs.langmuir.6b00693.

[41] P.M.P. Lins, V.S. Marangoni, T.M. Uehara, P.B. Miranda, V. Zucolotto, J. Cancino-Bernardi, Differences in the Aspect Ratio of Gold Nanorods that Induce Defects in Cell Membrane Models, Langmuir. (2017). https://doi.org/10.1021/acs.langmuir.7b03051.

[42] A.M. Almeida, O.N. Oliveira, P.H.B. Aoki, Role of Toluidine Blue-O Binding Mechanism for Photooxidation in Bioinspired Bacterial Membranes, Langmuir. (2019). https://doi.org/10.1021/acs.langmuir.9b03045.

[43] J.F.R. Kerr, C.M. Winterford, B. V. Harmon, Apoptosis. Its significance in cancer and cancer Therapy, Cancer. (1994). https://doi.org/10.1002/1097-0142(19940415)73:8<2013::AID-CNCR2820730802>3.0.CO;2-J.

[44] V.A. Fadok, D.R. Voelker, P.A. Campbell, J.J. Cohen, D.L. Bratton, P.M. Henson, Exposure of phosphatidylserine on the surface of apoptotic lymphocytes triggers specific recognition and removal by macrophages., J. Immunol. (1992).

[45] I. Vermes, C. Haanen, H. Steffens-Nakken, C. Reutellingsperger, A novel assay for apoptosis Flow cytometric detection of phosphatidylserine expression on early apoptotic cells using fluorescein labelled Annexin V, J. Immunol. Methods. (1995). https://doi.org/10.1016/0022-1759(95)00072-I.

[46] A.J. Schroit, R.F.A. Zwaal, Transbilayer movement of phospholipids in red cell and platelet membranes, BBA - Rev. Biomembr. 1071 (1991) 313–329. https://doi.org/10.1016/0304-4157(91)90019-S.

[47] P.F. Devaux, A. Zachowski, Maintenance and consequences of membrane

phospholipid asymmetry, Chem. Phys. Lipids. 73 (1994) 107–120. https://doi.org/10.1016/0009-3084(94)90177-5.
[48] T. Buffeteau, B. Desbat, J.M. Turlet, Polarization Modulation FT-IR Spectroscopy of Surfaces and Ultra-Thin Films: Experimental Procedure and Quantitative Analysis, Appl. Spectrosc. (1991). https://doi.org/10.1366/0003702914337308.
[49] R. Mendelsohn, G. Mao, C.R. Flach, Infrared reflection-absorption spectroscopy: Principles and applications to lipid-protein interaction in Langmuir films, Biochim. Biophys. Acta - Biomembr. (2010). https://doi.org/10.1016/j.bbamem.2009.11.024.
[50] R.F. Aroca, G.Y. Teo, H. Mohan, A.R. Guerrero, P. Albella, F. Moreno, Plasmon-Enhanced Fluorescence and Spectral Modification in SHINEF, J. Phys. Chem. C. 115 (2011) 20419–20424. https://doi.org/10.1021/jp205997u.
[51] M.B. Kobal, W.M. Pazin, M.J. Bistaffa, C.J.L. Constantino, K.A. Toledo, P.H.B. Aoki, Correlating Artepillin C cytotoxic activity on HEp-2 cells with bioinspired systems of plasma membranes, Mater. Sci. Eng. C. 112 (2020) 110943. https://doi.org/10.1016/j.msec.2020.110943.
[52] P. Meksiarun, P.H.B. Aoki, S.J. Van Nest, R.G. Sobral-Filho, J.J. Lum, A.G. Brolo, A. Jirasek, Breast cancer subtype specific biochemical responses to radiation, Analyst. (2018). https://doi.org/10.1039/C8AN00345A.
[53] P.S.S. Souza, L.V. Barbosa, L.F.A. Diniz, G.S. da Silva, B.R.P. Lopes, P.M.R. Souza, G.C. de Araujo, D. Pessoa, J. de Oliveira, F.P. Souza, K.A. Toledo, Neutrophil extracellular traps possess anti-human respiratory syncytial virus activity: Possible interaction with the viral F protein, Virus Res. (2018). https://doi.org/10.1016/j.virusres.2018.04.001.
[54] S. Sennato, F. Bordi, C. Cametti, C. Coluzza, A. Desideri, S. Rufini, Evidence of domain formation in cardiolipin-glycerophospholipid mixed monolayers. A thermodynamic and AFM study, J. Phys. Chem. B. (2005). https://doi.org/10.1021/jp051893q.
[55] J. Cancino-Bernardi, V.S. Marangoni, J.C.F. Besson, M.E.C. Cancino, M.R.M. Natali, V. Zucolotto, Gold-based nanospheres and nanorods particles used as theranostic agents: An in vitro and in vivo toxicology studies, Chemosphere. (2018). https://doi.org/10.1016/j.chemosphere.2018.09.012.
[56] K.A.T. Maria J. Bistaffa, Mirella B. Kobal, Priscila S. S. Souza, and P.H.B.A. Sabrina A. Camacho, Photo-Induced Necrosis on Oropharyngeal Carcinoma (HEp-2) Cells Mediated by the Xanthene Erythrosine, J. Nanosci. Nanotechnol. 20 (2020) 1533–4880. https://doi.org/10.1166/jnn.2020.18123.
[57] I.O. Osorio-Roman, A.R. Guerrero, P. Albella, R.F. Aroca, Plasmon Enhanced Fluorescence with Aggregated Shell-Isolated Nanoparticles, Anal. Chem. 86 (2014) 10246–10251. https://doi.org/10.1021/ac502424g.
[58] B. St-Louis Lalonde, É. Boulais, J.-J. Lebrun, M. Meunier, Visible and near infrared resonance plasmonic enhanced nanosecond laser optoporation of cancer cells, Biomed. Opt. Express. (2013). https://doi.org/10.1364/boe.4.000490.
[59] Y. Frión-Herrera, A. Díaz-García, J. Ruiz-Fuentes, H. Rodríguez-Sánchez, J. Maurício Sforcin, Mechanisms underlying the cytotoxic effect of propolis on human laryngeal epidermoid carcinoma cells, Nat. Prod. Res. (2018). https://doi.org/10.1080/14786419.2017.1363749.
[60] A.A. Torrano, Â.S. Pereira, O.N. Oliveira, A. Barros-Timmons, Probing the interaction of oppositely charged gold nanoparticles with DPPG and DPPC Langmuir monolayers as cell membrane models, Colloids Surfaces B Biointerfaces. 108 (2013) 120–126. https://doi.org/10.1016/j.colsurfb.2013.02.014.

[61] J.A.F. Op den Kamp, Lipid Asymmetry in Membranes, Annu. Rev. Biochem. (1979). https://doi.org/10.1146/annurev.bi.48.070179.000403.
[62] J.V.N. Ferreira, J.H.G. Lago, L. Caseli, Thymol in cellular membrane models formed by negative charged lipids causes aggregation at the air-water interface, Chem. Phys. Lett. (2019). https://doi.org/10.1016/j.cplett.2019.01.006.
[63] I. Zawisza, A. Lachenwitzer, V. Zamlynny, S.L. Horswell, J.D. Goddard, J. Lipkowski, Electrochemical and Photon Polarization Modulation Infrared Reflection Absorption Spectroscopy Study of the Electric Field Driven Transformations of a Phospholipid Bilayer Supported at a Gold Electrode Surface, Biophys. J. (2003). https://doi.org/10.1016/S0006-3495(03)74819-X.
[64] N. Hussein, C.C. Lopes, P.C.A. Pernambuco Filho, B.R. Carneiro, L. Caseli, Surface chemistry and spectroscopy studies on 1,4-naphthoquinone in cell membrane models using Langmuir monolayers, J. Colloid Interface Sci. (2013). https://doi.org/10.1016/j.jcis.2013.04.005.
[65] Q. Huo, L. Dziri, B. Desbat, K.C. Russell, R.M. Leblanc, Polarization-Modulated Infrared Reflection Absorption Spectroscopic Studies of a Hydrogen-Bonding Network at the Air-Water Interface, J. Phys. Chem. B. (1999). https://doi.org/10.1021/jp984389c.
[66] I.W. Levin, T.E. Thompson, Y. Barenholz, C. Huang, Two Types of Hydrocarbon Chain Interdigitation in Sphingomyelin Bilayers, Biochemistry. (1985). https://doi.org/10.1021/bi00343a036.
[67] R.A. Vaia, R.K. Teukolsky, E.P. Giannelis, Interlayer Structure and Molecular Environment of Alkylammonium Layered Silicates, Chem. Mater. (1994). https://doi.org/10.1021/cm00043a025.
[68] A. Gericke, C.R. Flach, R. Mendelsohn, Structure and orientation of lung surfactant SP-C and L-α- dipalmitoylphosphatidylcholine in aqueous monolayers, Biophys. J. (1997). https://doi.org/10.1016/S0006-3495(97)78087-1.
[69] J. Madejová, ˛udmila Sekeráková, V. Bizovská, M. Slaný, ˛uboš Jankovič, Near-infrared spectroscopy as an effective tool for monitoring the conformation of alkylammonium surfactants in montmorillonite interlayers, Vib. Spectrosc. (2016). https://doi.org/10.1016/j.vibspec.2016.02.010.
[70] H. Akutsu, T. Nagamori, Conformational Analysis of the Polar Head Group in Phosphatidylcholine Bilayers: A Structural Change Induced by Cations, Biochemistry. (1991). https://doi.org/10.1021/bi00232a020.
[71] M.C. Wiener, S.H. White, Structure of a fluid dioleoylphosphatidylcholine bilayer determined by joint refinement of x-ray and neutron diffraction data. III. Complete structure, Biophys. J. (1992). https://doi.org/10.1016/S0006-3495(92)81849-0.
[72] L.R.S. Barbosa, W. Caetano, R. Itri, P. Homem-De-Mello, P.S. Santiago, M. Tabak, Interaction of phenothiazine compounds with zwitterionic lysophosphatidylcholine micelles: Small angle X-ray scattering, electronic absorption spectroscopy, and theoretical calculations, J. Phys. Chem. B. (2006). https://doi.org/10.1021/jp056486t.
[73] George Socrates, Infrared and Raman Characteristic Group Frequencies, John Wiley & Sons, Ltd, England, 2001.
[74] D. Blaudez, T. Buffeteau, N. Castaings, B. Desbat, J.M. Turlet, Organization in pure and alternate deuterated cadmium arachidate monolayers on solid substrates and at the air/water interface studied by conventional and differential Fourier transform infrared spectroscopies, J. Chem. Phys. (1996). https://doi.org/10.1063/1.471726.
[75] R.A. Dluhy, D.G. Cameron, H.H. Mantsch, R. Mendelsohn, Fourier Transform Infrared Spectroscopic Studies of the Effect of Calcium Ions on

Phosphatidylserine, Biochemistry. (1983). https://doi.org/10.1021/bi00295a043.
[76] X. Chen, Z. Huang, W. Hua, H. Castada, H.C. Allen, Reorganization and caging of DPPC, DPPE, DPPG, and DPPS monolayers caused by dimethylsulfoxide observed using brewster angle microscopy, Langmuir. (2010). https://doi.org/10.1021/la102842a.
[77] J.F.D. Liljeblad, V. Bulone, E. Tyrode, M.W. Rutland, C.M. Johnson, Phospholipid monolayers probed by vibrational sum frequency spectroscopy: Instability of unsaturated phospholipids, Biophys. J. (2010). https://doi.org/10.1016/j.bpj.2010.02.009.
[78] P.J. Gomes, A.M.P.S. Gonçalves Da Silva, P.A. Ribeiro, O.N. Oliveira, M. Raposo, Radiation damage on Langmuir monolayers of the anionic 1.2-dipalmitoyl-sn-glycero-3-[phospho-rac-(1-glycerol)] (sodium salt)(DPPG) phospholipid at the air-DNA solution interface, Mater. Sci. Eng. C. (2016). https://doi.org/10.1016/j.msec.2015.09.017.
[79] E. González-Labrada, R. Schmidt, C.E. DeWolf, Kinetic analysis of the ozone processing of an unsaturated organic monolayer as a model of an aerosol surface, Phys. Chem. Chem. Phys. (2007). https://doi.org/10.1039/b707890k.
[80] L. Qiao, A. Ge, M. Osawa, S. Ye, Structure and stability studies of mixed monolayers of saturated and unsaturated phospholipids under low-level ozone, Phys. Chem. Chem. Phys. (2013). https://doi.org/10.1039/c3cp52484a.
[81] H.S. Jung, J. Han, J.H. Lee, J.H. Lee, J.M. Choi, H.S. Kweon, J.H. Han, J.H. Kim, K.M. Byun, J.H. Jung, C. Kang, J.S. Kim, Enhanced NIR radiation-triggered hyperthermia by mitochondrial targeting, J. Am. Chem. Soc. (2015). https://doi.org/10.1021/ja5122809.
[82] T.A. Dix, J. Aikens, Mechanisms and Biological Relevance of Lipid Peroxidation Initiation, Chem. Res. Toxicol. (1993). https://doi.org/10.1021/tx00031a001.
[83] T.L. Eliason, J.B. Gilman, V. Vaida, Oxidation of organic films relevant to atmospheric aerosols, Atmos. Environ. (2004). https://doi.org/10.1016/j.atmosenv.2003.11.025.
[84] D. Trachootham, J. Alexandre, P. Huang, Targeting cancer cells by ROS-mediated mechanisms: A radical therapeutic approach?, Nat. Rev. Drug Discov. (2009). https://doi.org/10.1038/nrd2803.
[85] J. Wong-Ekkabut, Z. Xu, W. Triampo, I.M. Tang, D.P. Tieleman, L. Monticelli, Effect of lipid peroxidation on the properties of lipid bilayers: A molecular dynamics study, Biophys. J. (2007). https://doi.org/10.1529/biophysj.107.112565.
[86] A. Catalá, An overview of lipid peroxidation with emphasis in outer segments of photoreceptors and the chemiluminescence assay, Int. J. Biochem. Cell Biol. (2006). https://doi.org/10.1016/j.biocel.2006.02.010.
[87] U.P. Fringeli, The Structure of Lipids and Proteins Studied by Attenuated Total Reflection (ATR) Infrared Spectroscopy: II. Oriented Layers of a Homologous Series: Phosphatidylethanolamine to Phosphatidylcholine, Zeitschrift Fur Naturforsch. - Sect. C J. Biosci. (1977). https://doi.org/10.1515/znc-1977-1-205.
[88] T.F. Schmidt, L. Caseli, O.N. Oliveira, R. Itri, Binding of methylene blue onto langmuir monolayers representing cell membranes may explain its efficiency as photosensitizer in photodynamic therapy, Langmuir. 31 (2015) 4205–4212. https://doi.org/10.1021/acs.langmuir.5b00166.